Pion production in the reaction $d(p;d,\pi)n$ at 800 MeV with a spectator neutron

J. W. Lo, E. V. Hungerford, J. C. Allred, B. W. Mayes, L. S. Pinsky, M. L. Warneke, and T. M. Williams
University of Houston, Houston, Texas 77004

J. M. Clement, W. H. Dragoset, R. D. Felder, J. H. Hoftiezer, J. Hudomalj-Gabitzsch, G. S. Mutchler, and G. C. Phillips
T. W. Bonner Nuclear Laboratories, Rice University, Houston, Texas 77001
(Received 23 February 1979)

The differential cross section for the $pd \rightarrow d\pi^+ n$ reaction at 800 MeV was measured in a kinematically complete experiment in regions of phase space where the neutron in the target deuteron recoils with near zero momentum. It was observed that the reaction basically proceeds through a quasifree process where the neutron is a spectator to the $pp \rightarrow d\pi$ reaction. A calculation using the simple spectator model predicts the measured cross section when the neutron recoil momentum is near zero. At neutron recoil momenta of about 100 MeV/c, the cross section is approximately 35% lower than the data.

[NUCLEAR REACTIONS ^{2}H$(p,d\pi^+)n$, $E=800$ MeV; measured $\sigma(P_d, \theta_d, \theta_\pi)$ model with spectator neutron. Deduced validity of spectator model.]

I. INTRODUCTION

Pion production induced by nucleons on light nuclei has been a subject of continuing interest. In the past 25 years a vast amount of data[1-9] has been obtained, covering a wide range of energies. There also has been a considerable amount of theoretical work[10-20] devoted to the pion production mechanism. However, pion production by protons incident on a deuterium target is particularly interesting. In this reaction the inclusive pion production at 730 MeV (Ref. 9) was found to be less than the sum of the inclusive pion production from protons on protons and protons on neutrons. This was attributed to a Glauber shadowing process or a strong interference.

Figure 1 shows spectra at two angles from the data of Cochran *et al.*[9] for inclusive positive pion production from hydrogen and deuterium. Positive pion production from a deuterium target is seen to be consistently lower than pion production from hydrogen, especially at forward angles and for higher pion energies. The magnitude of the effect is such that if the deuteron is treated as an independent proton and neutron, the amplitudes for $pp \rightarrow \pi^+ X$ and $pn \rightarrow \pi^+ X$ must be about 120° out of phase. If the cross section includes only simple Glauber shadowing with no interference, it may be expressed as

$$\sigma_d = \sigma_p + \sigma_n - \frac{\sigma_p \sigma_n}{4\pi \langle r^2 \rangle} . \quad (1)$$

However, this equation cannot be satisfied with the measured cross sections and known deuteron radius.

At 800 MeV one would expect a large contribution to the cross section from quasifree processes. Therefore, it is important to investigate nucleon-deuteron pion production in specific reaction channels with complete kinematics. We report here on pion production from deuterium in the kinematic region when the neutron in the deuteron should remain a spectator to the process as described in Fig. 2(a).

To place this paper in proper perspective, some of the previous work will be summarized. Measurement of the differential cross section for the

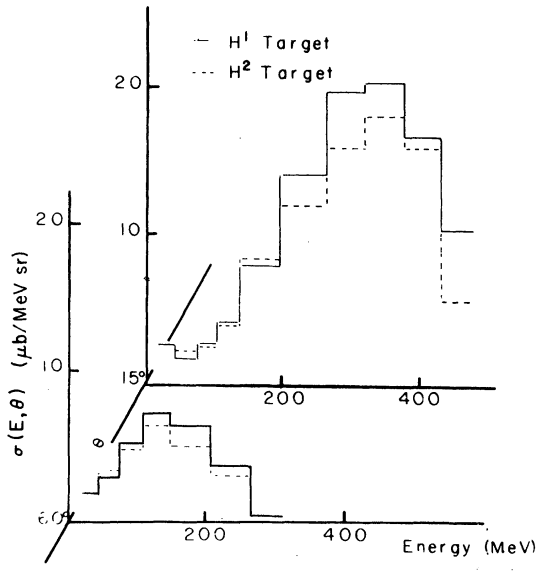

FIG. 1. Inclusive pion production cross sections at 15° and 60° from the data of Cochran *et al.*, Ref. 9.

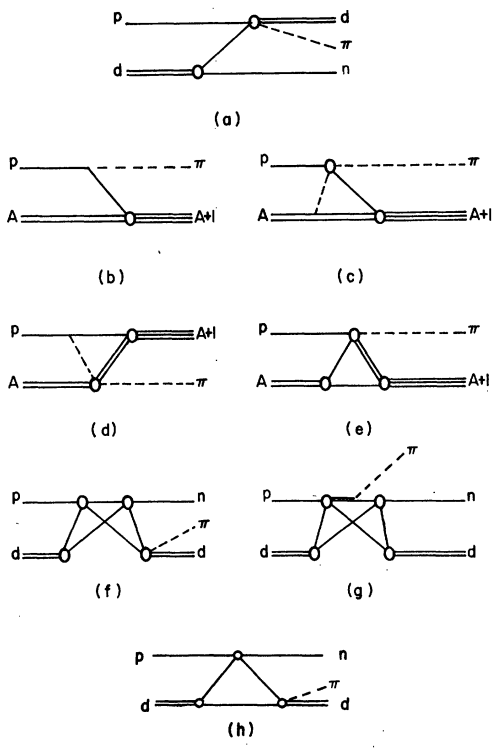

FIG. 2. Feynman diagrams for several pion production processes. (a) Neutron Spectator Model (SM), (b) single nucleon pickup mechanism (SNM), (c) and (d) double nucleon pickup mechanism (DNM), (e) plane wave impulse approximation, (f) and (g) double Glauber scatter mechanism, and (h) Ruderman model.

$\pi^+ d \to pp$ reaction was made at pion energies between 152 and 262 MeV by Richard-Serre *et al.*[1] Assuming the validity of detailed balance, this reaction is equivalent to the $pp \to d\pi$ reaction for incident proton energies between 570 and 810 MeV. The data have been fitted quite well to the form

$$\frac{d\sigma^{\rm cm}}{d\Omega_\pi} = K(A + \cos^2\theta_\pi - B\cos^4\theta_\pi). \quad (2)$$

The first two terms account for the production of s and p wave pions while the $\cos^4\theta$ provides for the production of d and f wave pions. More recently at Los Alamos Meson Physics Facility (LAMPF),[3] some 800 MeV $pp \to d\pi$ data were obtained and Eq. (2) was fitted to the data. For energies between 1 and 4.1 GeV, the $pp \to d\pi^+$ angular distributions were measured by Heinz[4] and Anderson.[5] It was found that for $T_p > 1.3$ GeV, the maximum near the forward angles is pronounced which makes fitting the differential cross section with up to $\cos^8\theta$ terms necessary.

The $pd \to d\pi^+ n$ reaction at 585 MeV was studied by Hogstrom *et al.*[8] at neutron recoil momentum greater than 400 MeV/c. Duck *et al.*[20] have had reasonable success with a double scattering Glauber theory where the shape of the data is fitted with the $pp \to d\pi$ amplitude [see Fig. 2(h)], but inclusion of double scattering diagrams of the form given in Figs. 2(f) and 2(g) is necessary to predict the overall magnitude.

In view of the success of the distorted wave impulse approximation (DWIA) and the spectator model (SM) applied to the $pd \to ppn$ reaction by Witten *et al.*[21] at 585 MeV and Felder *et al.*[3] at 800 MeV, this experiment was initiated to measure the $pd \to d\pi^+ n$ reaction in a kinematic region where the neutron may remain a spectator to the reaction. Since the data of Cochran *et al.*[9] show that the cross section for the inclusive π production from deuterium is less than the inclusive pion production from hydrogen, a measurement of pion production from deuterium into specific reaction channels is particularly desirable. Previous studies of the $pd \to d\pi^+ n$ reaction have included some unpublished experimental results of Bonner *et al.*[22] and interpretation of these data by Silbar.[23]

This paper is arranged so that in Sec. II the experimental layout and the data acquisition technique will be discussed. Data analysis and reduction will be covered in the next section. The experimental results compared to the predictions of the SM are presented in Sec. IV.

II. EXPERIMENTAL SETUP

A. General

This experiment was performed at LAMPF using the 800 MeV external proton beam (EPB). The physical layout of the experiment (see Fig. 3) was designed to optimize data collection for several reactions. As a result, the central ray of the spectrometer arm was limited to angles greater than 13.6°. The deuteron was detected in the spectrometer arm (MAGARM) measuring the momentum (P_d), scattering angle ($\hat{r}_d$), and pion velocity (β_π). Since the set of quantities ($P_d, \beta_d, \hat{r}_d, \hat{r}_\pi$) completely and uniquely define the $pd \to d\pi n$ event, this is a kinematically complete experiment. The angle pairs chosen for the observation of the reaction are near the kinematic region in the phase space where the neutron recoils with the least possible momentum. That is, the arms were set near the deuteron and pion scattering angles for the $pp \to d\pi$ reaction at 800 MeV.

B. Beam, target, and normalization

The LAMPF EPB has kinetic energy equal to 800 ± 0.1 MeV. The beam size at the target, as determined by the origin of the trajectories of

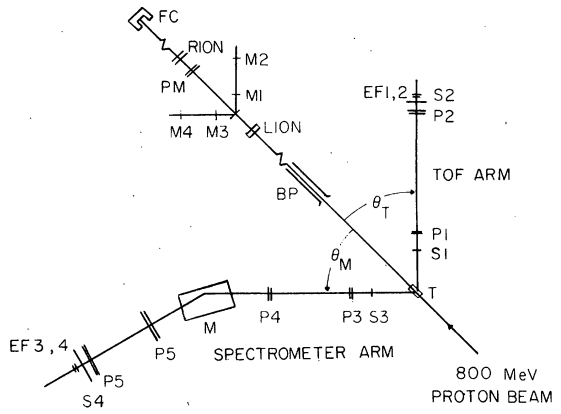

FIG. 3. Experimental layout for the detection of $pd \rightarrow d\pi^+ n$ reaction. The abbreviations are as follows: $S1$ to $S4$, scintillator counters; $P1$ to $P6$, multiwire proportional counters; M, the spectrometer magnet; T, the LD_2 target; $M1$–$M4$, monitor scintillator telescopes; PM, the beam profile monitor; RION the argon gas ion chamber; and FC, the Faraday cup.

the scattered particles, has a full width at half-maximum (FWHM) less than 3 mm vertically and less than 4 mm horizontally. Observing the glowing beam spot at the fluorescent screen inserted near the target confirmed this result, and therefore verified that the cross sectional area of the beam is well within that of the target. The beam current was typically ~10 pA (~6×10^7 protons/sec).

The target is 99.8% LD_2 in a kapton ($C_{22}H_{10}N_2O_5$) cylinder with hemispherical ends. The dimensions of the cylinder are length = 6.05 cm, diameter = 2.54 cm, and wall thickness = 0.013 (5/mil). The target cylinder was placed inside a 10^{-5} μm vacuum jacket. The LD_2 was liquified and kept in liquid state by a cryogenic refrigeration system.[24] The system kept the target temperature at 25 ± 1.5° K, and the target equilibrium pressure was 13.5 ± .5 psi (absolute). This results in the target density of 0.165 ± 0.004 g/cm^3. Multiple scattering of the deuteron in the target (LD_2, target cylinder, vacuum jacket) gives a maximum rms angle of less than 0.3°.

The beam monitoring system consisted of four components: a profile monitor (PM), a scintillation telescope monitor (M1–M4), an argon gas ion chamber (RION), and a Faraday cup (FC). The locations of each monitor are, respectively, 9.5 m, 9.7 m, 10 m, 19.7 m downstream from the target. The PM is an 8.1 × 8.1 cm^2 multiwire proportional counter (MWPC) with integrating readout ability.[25] It provided a convenient way to steer and focus the beam. The beam size at the PM is less than 3.2 cm. The M1–M4 monitor consisted of a 0.8 cm CH_2 target and two scintillation telescopes each consisting of two scintillation paddles. The telescope arms were placed at 40° on both sides of the beam. RION and the monitor telescope were calibrated with the FC between 10–300 pA.[3] RION gain was 158 ± 8 at the operating temperature and pressure. The FC, which was provided by LAMPF, has an effective aperture of 15.2 cm in diameter. With the beam divergence in the present experiment, all protons are believed to be collected by the cup. The uncertainty in the absolute beam normalization, which affects all cross sections equally, is estimated to be ±8%.

C. Detector arms

The time-of-flight (TOFARM) arm consisted of two scintillators S_1, S_2, two multiwire proportional counters (MWPC) P_1, P_2, and a set of efficiency scintillators EF_1 and EF_2 (see Fig. 3). The dimensions of S_1, P_1, P_2, and S_2 were chosen to subtend similar solid angles. The pulse height of a production pion was sensed at S_1. The trajectory of the pion can be traced using the entrance position recorded by P_1 and exit position recorded by P_2. The distance between S_1 and S_2 is 2.2 m. The efficiency of both S_1 and S_2 were checked by EF_1 and EF_2.

Except for the spectrometer magnet and one more pair of MWPC's, the MAGARM operated similarly to the TOFARM. The scintillator S_3 gave the pulse height of the traversing particle, and the time-of-flight of the particle was measured between S_3 and S_4. The efficiency of both S_3 and S_4 was checked by EF_3 and EF_4. The magnet had a pole tip dimension of 45.7 cm × 91.4 cm and a gap of 15 cm. A Monte Carlo calculation shows the momentum acceptance of the magnet is −25% to +30% of the central momentum. For the pd elastic run at the beginning of the experiment, the momentum resolution was 2.1 to 1.5% over a range of 940 to 1290 MeV/c. The angular resolution was found to be approximately 0.5°.

D. Electronic logic and data acquisition technique

The scintillators S_2, S_3, and S_4, in coincidence, provided a master trigger to enable the MWPC, P_1 through P_6. The scintillators S_1, S_2, and S_4 also produced two fast timing signals which measured the time-of-flight of the production particles in both arms. In addition, S_1 and S_3 also provided pulse height signals. The TOF's and pulse heights, together with the P_1-P_6 coordinates, were read through the dataway of a CAMAC interface into the data acquisition computer.[26] All the data were immediately written on a magnetic tape. In addition, part of the data was analyzed on-line for

monitoring purposes. The *I/O* operation was completely handled by a microprogrammed input-output processor,[27] while the PDP 11/45 was responsible for the on-line analysis.

III. DATA ANALYSIS

A. Introduction

Kinematically complete measurements of the three-body reaction $pd \to d\pi^+ n$ can be used to determine the fifth order differential cross section. The following formula was used to calculate the experimental average of this cross section:

$$\overline{\sigma(P_d, \theta_d, \theta_\pi)}\big|_R = \frac{DET/(TDE \cdot DT)}{I \cdot \eta \cdot [\Omega_d \Omega_\pi(R)]_{MC} \cdot \Delta P_d} . \quad (3)$$

Here R is the region over which the experimental average was calculated. If one defines $\Omega_i(\hat{x}_i)$ to be a solid angle of size Ω_i about a central direction $\hat{x}_i$, then an event defined by $(P_d, \beta_d, \hat{r}_d, \hat{r}_\pi)$ is said to be in R if $\hat{r}_i$ is within $\Omega_i(\hat{x}_i)$ for $i = d$, π, and P_d between P and $P + \Delta P$. The term DET is the number of good $pd \to d\pi^+ n$ events detected in R, and TDE and DT are the MWPC system data efficiency and total system dead-time correction, respectively. The determination of DET, TDE, and DT will be discussed in the next subsection. The term I is the number of incident protons, η is the number of target nuclei per cm^2 (0.316×10^{-24}), and $[\Omega_d \Omega_\pi(R)]_{MC}$ is calculated by a Monte Carlo method discussed in part C.

B. Event identification and system efficiency

A good event is defined by the following criteria: (1) The product deuteron and pion pair must have trajectories which when projected backward intersect within the dimensions of the target. The X and Y target distributions were Gaussian with a FWHM of about 7.6 mm. The Z target distribution was rectangular and equal to the target length of 61 mm. The widths of the X, Y, and Z cuts were 25, 25, and 89 mm, respectively. (2) The pulse height of an event in the TOFARM and MAGARM must correspond to the proper pion and deuteron pulse height, respectively. (3) The measured TOF of a particle and its calculated value must agree within the width of the system TOF resolution which was approximately 2 nsec (FWHM). The TOF cut was 6 nsec wide centered on the TOF peak. (4) The product deuteron must possess a measured trajectory corresponding to the calculated one when entering the magnet and leaving the magnet. The calculated trajectory is obtained by using the measured p_d and propagating the deuteron through the magnet assuming a uniform field. Matching the projected and actual positions of the particle at $P5$ produced a distribution in position about 9 mm wide (FWHM) both horizontally and vertically. Cuts on these distributions were selected to pass all valid events. The deuteron must also enter within the valid pole gap of the magnet. (5) The particle transversing through the MAGARM must have mass corresponding to a deuteron, and the particle in the TOFARM must have a time-of-flight for a pion obeying the kinematics for the $pd \to d\pi^+ n$ reaction. With the above criteria, accidentals and background events were, in practice, removed. The ratio of good to bad events was approximately 0.5. The good events are binned in a two-dimensional array of P_d vs θ_d.

The efficiency of the scintillators S_1 to S_4 is unity from previous experience[2] and from the efficiency monitors. The efficiency for the MWPC systems P_1-P_6 is calculated only for those events which had TOF and pulse height corresponding to a $pd \to d\pi^+ n$ reaction. In this way, the efficiency of the system for detecting particles of the appropriate velocities and charges was determined. The data efficiency for the entire MWPC system is given by

$$TDE = GD/(GD + BD) ,$$

where GD is the total number of events for which each coordinate of the MWPC system had one and only one readout, and BD is the total number of events that are not "good." The DT of the system is calculated by comparing the free running monitor events to the same events gated by the system dead time. Corrections for pileup and accidental events were included.

C. Solid angle

With a finite size target, multiple detectors on each arm, a spectrometer magnet, energy loss, multiple scattering, and three-body kinematics, the solid angles of the experimental system are not easy to calculate analytically. Therefore a Monte Carlo method was used. Applying it to the present case, one has

$$[\Omega_d \Omega_\pi(R)]_{MC} = \Omega_d^{Try} \cdot \Omega_\pi^{Try} \times \frac{PASS(R)}{TRY(R)} ,$$

where Ω_i^{Try} is the solid angle defined by R, into which the ith particle is projected, $TRY(R)$ is the number of events tried which had $(P_d, \beta_d, \hat{r}_d, \hat{r}_\pi)$ inside R, and $PASS(R)$ in the number of events in R that successfully passed through the respective arms.

To determine $PASS(R)$, a computer program MC3 simulating the present experiment, was written to follow this sequence: (1) Randomly choose the $(P_d, \hat{r}_d, \hat{r}_\pi)$ of an event from a momentum range corresponding to the momentum acceptance of the

appropriate magnet setting, and from solid angles bigger than the solid angles subtended by the detector arms. (2) Check whether if the $(P_d, \hat{r}_d, \hat{r}_\pi)$ chosen satisfies the three-body kinematics. (3) Randomly choose a scattering origin and propagate the d and π down the respective arms including energy loss, multiple scattering, and π decays via the $\pi \to \mu\nu$ mode. (4) If both particles are successfully transmitted through the arms, bin this passed event in a two-dimensional array of P_d vs θ_d. Repeat this sequence until statistics are sufficiently accurate.

Figure 4 is a Monte Carlo calculation of the experimental acceptance $[\Omega_d \Omega_\pi(R)]_{MC}$ for the angles $\theta_{MAG} = 15°$ and $\theta_{TOF} = 40°$ as a function of momentum only, for the convenience of graphic representation.

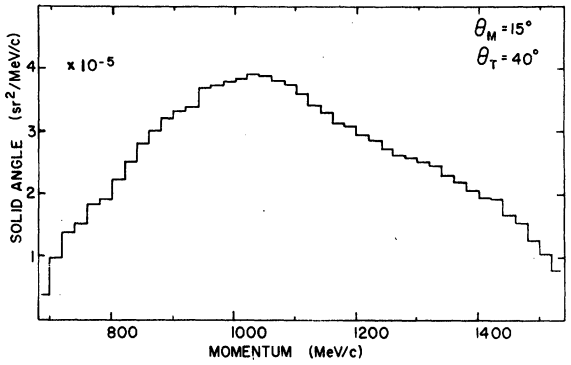

FIG. 4. Solid angle of the experimental apparatus plotted as a function of deuteron momentum for an angular setting of $\theta_{MAG} = 15°$, $\theta_{TOF} = 40°$.

D. Spectator model

The experimental data were analyzed in terms of the simple spectator model SM. In the SM the three-body lab cross section can be written as[21]

$$\sigma(P_d, \theta_d, \theta_\pi) = K \cdot |\phi_d(P_n)|^2 \cdot \sigma(\theta_\pi)_{pp \to d\pi^+},$$

The kinematic factor K is equal to the product of the three-body Lorentz invariant phase space and the two-body CM lab Jacobian. It is given by

$$K = \left(\frac{p_d^2 p_\pi^2}{E_d(P_\pi E_n - E_\pi \vec{P}_n \cdot \hat{P}_\pi) p_p} \right)^{3B} \left(\frac{p_p^* S}{p_\pi^*} \right)^{2B}. \quad (4)$$

Here the superscript $3B$ stands for the kinematic variable calculated with the $pd \to d\pi^+ n$ kinematics for the event defined by $(P_d, \hat{r}_d, \hat{r}_\pi)$. In this notation, E is the relativistic total energy and P is the corresponding three momentum. The $2B$ stands for variables calculated with the $pp \to d\pi^+$ kinematics for which the target proton is assumed to have $\vec{P}_p$ equal to $-\vec{P}_n$. The asterisk denotes c.m. quantities and S is the invariant squared mass of the two-body system. The symbol $\phi_d(P_n)$ is the momentum wave function of the target deuteron evaluated at the spectator neutron momentum P_n. The deuteron wave function chosen here is the Moravcsik[28] approximation III of the Gartenhaus deuteron wave function. The Fourier transform of the appropriately normalized s-wave function is

$$\phi^s(k) = a \sum_{j=1}^{8} \frac{(-1)^{j+1}}{b_j^2 + k^2} \text{ fm}^{3/2},$$

where k is the proton-neutron relative momentum expressed in fm^{-1}; $a = 0.630/\pi$; b_i for $i = 1, 8$ are 0.232, 1.82, 2.73, 4.32, 1.90, 3.59, 4.40, and 5.99. Comparing ϕ^s with the complete Gartenhaus deuteron wave function in momentum representation shows that ϕ^s is sufficiently accurate out to $k \leq 200$ MeV/c, which overlaps the P_n range of the present experiment. The symbol $\sigma(\theta_\pi)_{pp \to d\pi^+}$ represents the c.m. differential cross section for the $pp \to d\pi^+$ reaction at θ_π^* for a given c.m. energy $\sqrt{S}$. An analytical form of $\sigma(\theta_\pi)_{pp \to d\pi^+}$ was obtained by assuming the form given in Eq. (2) and fitting it to the data in Ref. 1. Letting A and B be constant and K be proportional to the total cross section, one obtains

$$A = 0.26,$$

$$B = 0.43,$$

$$C = 1.842 \times 10^4/(1 + 0.005\,74\ T_p)\ \mu\text{b/sr},$$

where T_p is the equivalent incident proton kinetic energy in MeV for a $pp \to d\pi^+$ system where the target proton is at rest. It should be noted that the fit was performed only over the experimental angular and energy ranges $\theta_\pi^* = [24°, 85°]$, $T_p = [680, 930$ MeV$]$, so that more accurate fits could be obtained.

The experimental average of the cross section predicted by the SM can be calculated using the Monte Carlo method and it gives

$$\overline{\sigma(P_d, \theta_d, \theta_\pi)}|_R = \frac{\sum_{\text{Events}} \sigma(P_d, \theta_d, \theta_\pi) (\text{of the passed events})}{\text{Number of passes}}. \quad (5)$$

A comparison of the results obtained from Eqs. (5) and (3) is given in the next section.

IV. RESULTS

To ensure proper normalization, the *pd* elastic cross section was measured using the present material setup. The results agrees well with previous *pd* elastic data taken independently.[29] Although published values of elastic *pd* cross sections at 800 MeV do not exist, elastic *pp* data obtained under the same conditions[3] as the earlier *pd* data duplicate the data of Willard *et al.*[30]

The results of the analysis of the $pd \to d\pi^+ n$ reaction in the kinematic region where the neutron recoil momentum P_n can vanish are given in Table I and Fig. 5. The error bars on the data points

TABLE I. Tabulated values of the cross section as a function of deuteron momentum and angle for the reaction $pd \to d\pi n$ at 800 MeV. The symbols θ_M/θ_T represent the angles of the spectrometer arm and time-of-flight arm, and P_d represents the deuteron momentum.

P_d (MeV/c)	Exp (μb/sr^2-MeV/c)	SM	Exp (μb/sr^2-MeV/c)	SM	Exp (μb/sr^2-MeV/c)	SM
θ_M/θ_T	11.2°/20°		12.8°/25°		13.9°/30°	
two-body P_d	980 (MeV/c)		1020 (MeV/c)		1060 (MeV/c)	
two-body θ_d/θ_π	13.7°/20.4°		13.7°/25°		13.7°/30°	
800	6.47 ± 0.76	2.49				
820	8.71 ± 0.86	4.72				
840	15.2 ± 1.1	9.21	1.09 ± 0.31	1.23		
860	25.4 ± 1.5	17.7	6.10 ± 0.70	4.36		
880	41.9 ± 2.0	35.5	13.5 ± 1.0	8.38	2.76 ± 0.60	1.24
900	63.2 ± 2.5	52.3	23.9 ± 1.3	16.9	4.26 ± 0.54	2.53
920	101.0 ± 3.3	101	47.6 ± 1.9	33.8	6.58 ± 0.65	5.46
940	124.0 ± 3.7	113	73.3 ± 2.4	59.3	14.9 ± 0.97	10.4
960	132.0 ± 3.9	121	116.0 ± 3.1	95.5	26.7 ± 1.3	21.5
980	109.0 ± 3.4	125	158.0 ± 3.7	144	46.2 ± 1.7	41.3
1000	72.8 ± 2.7	115	176.0 ± 4.1	163	82.7 ± 2.4	70.7
1020	55.0 ± 2.4	76.0	150.0 ± 3.6	164	124.0 ± 3.1	108
1040	34.2 ± 1.8	39.9	118.0 ± 3.2	135	150.0 ± 3.5	146
1060	21.3 ± 1.5	24.3	80.1 ± 2.6	94.6	148.0 ± 3.4	148
1080	13.2 ± 1.2	17.2	54.4 ± 2.1	59.3	122.0 ± 3.1	132
1100			31.8 ± 1.7	35.5	90.8 ± 2.6	96.9
1120			19.8 ± 1.3	21.0	60.2 ± 2.0	63.8
1140			12.2 ± 1.0	13.0	38.7 ± 1.7	39.9
1160			8.15 ± 0.87	7.41	20.7 ± 1.2	23.5
1180			4.84 ± 0.68	4.56	12.9 ± 0.97	13.5
1200					7.93 ± 0.76	7.67
θ_M/θ_T	14.4°/35°		14.7°/40°		14.6°/45°	
two-body P_d	1119 (MeV/c)		1151 (MeV/c)		1210 (MeV/c)	
two-body θ_d/θ_π	13.7°/35°		13.7°/40°		14.7°/45°	
940	3.42 ± 0.65	1.24				
960	5.79 ± 0.83	2.75				
980	10.8 ± 1.2	5.74	1.34 ± 0.24	0.64		
1000	22.0 ± 1.7	12.4	3.36 ± 0.39	1.23		
1020	38.2 ± 2.3	22.4	4.77 ± 0.46	2.96		
1040	67.0 ± 3.1	44.9	11.1 ± 0.71	5.75	2.28 ± 0.28	0.92
1060	95.1 ± 3.8	68.7	17.8 ± 0.89	13.6	3.07 ± 0.33	1.87
1080	119.0 ± 4.4	110	35.5 ± 1.3	25.7	6.66 ± 0.49	3.92
1100	128.0 ± 4.7	132	58.6 ± 1.7	45.3	12.6 ± 0.68	8.33
1120	109.0 ± 4.3	121	83.4 ± 2.1	76.6	25.6 ± 1.0	16.9
1140	84.2 ± 3.7	94.6	96.5 ± 2.4	92.0	47.3 ± 1.4	32.7
1160	58.1 ± 3.1	62.7	92.9 ± 2.3	96.9	68.9 ± 1.8	54.7
1180	34.0 ± 2.3	35.3	68.3 ± 2.0	75.2	85.5 ± 2.1	71.8
1200	20.1 ± 1.8	23.3	44.5 ± 1.6	50.2	79.8 ± 2.1	75.2
1220	11.6 ± 1.4	12.1	27.4 ± 1.2	26.2	54.4 ± 1.7	56.7
1240	6.27 ± 1.0	6.72	15.9 ± 0.93	17.1	32.4 ± 1.3	32.2
1260	3.51 ± 0.79	3.98	7.21 ± 0.63	8.55	17.0 ± 0.92	15.9
1280			4.65 ± 0.50	4.44	9.92 ± 0.72	7.64
1300			3.77 ± 0.46	2.13	3.78 ± 0.44	3.64
1320					2.47 ± 0.37	1.80

are statistical uncertainties, and the solid line histograms are the differential cross sections calculated using the SM discussed in the previous section. No adjustment of normalization has been made to improve the fit. The fifth order differential cross sections shown here have been averaged over the entire solid angle of both the TOF arm and the MAG arm so that they may be expressed as functions of P_d only. Strong peaks centered near $P_n = 0$ are still observed.

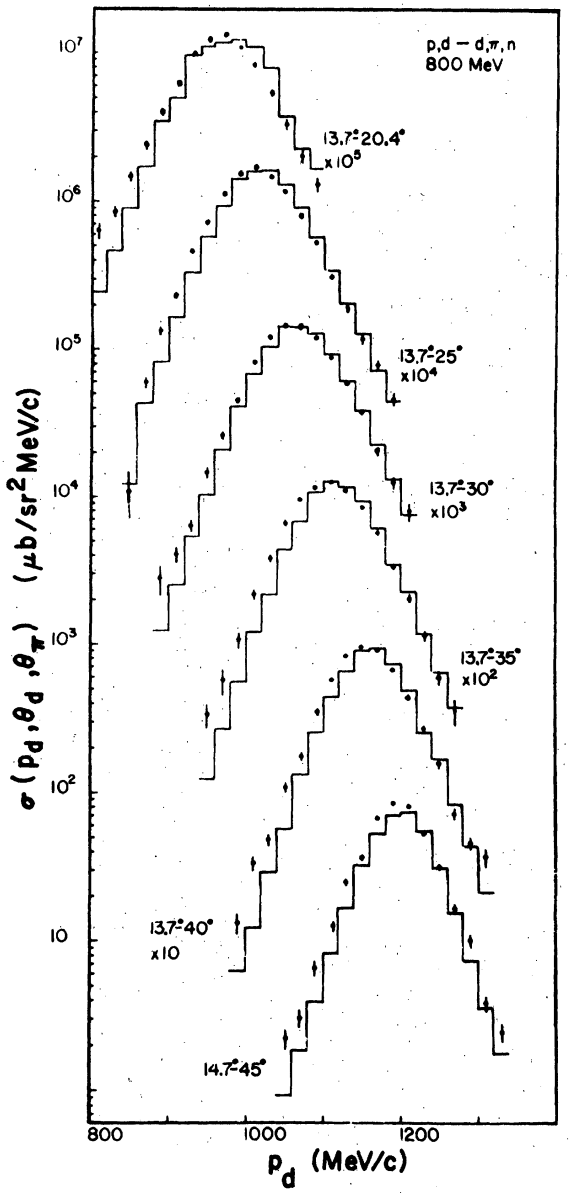

FIG. 5. The cross section of $\sigma(P_d, \theta_d, \theta_\pi)$ as a function of deuteron momentum P_d, for the reaction $pd \rightarrow d\pi^+ n$ at 800 MeV. The angles of the detector arms were positioned on the $pp \rightarrow d\pi$ kinematic locus. Only statistical errors are shown. The histograms are predictions of the spectator model for each angle setting. Each spectrum is labeled by the spectrometer and time-of-flight arm angles, written θ_{MAG}-θ_{TOF}.

The cross section $\sigma(P_d, \theta_d, \theta_\pi)$ is relatively constant over the pion solid angle, but it varies quite rapidly (two orders of magnitude) within the experimental range of deuteron momentum and the solid angle of the spectrometer arm. Therefore it is more meaningful to show the cross section as a function of two variables P_d and $\Delta\theta_d$, where $\Delta\theta_d$ is the difference in the deuteron angle determined by using the averaged pion angle in the two-body kinematics for $pp \rightarrow d\pi^+$ and the observed deuteron angle. An example of this is shown in Fig. 6, where the angle setting of the detector arms was $\theta_{MAG}/\theta_{TOF} = 13.7°/30°$. The error bars are not shown in the figure for simplicity, but they range from ±6% at the peak in the cross section to approximately ±30% at the lowest measured values. For a pion scattered at 30° in a $pp \rightarrow d\pi^+$ reaction, the corresponding scattering angles and momentum for the deuteron are 13.8° and 1065 MeV/c. If the $pd \rightarrow d\pi^+ n$ reaction proceeds predominantly through the quasifree mechanism [Fig. 2(a)], one expects the fifth order cross section to peak at the two-body kinematic locus of deuteron and pion angles. This is found to be the case for all results where the neutron can kinematically remain at rest in the lab system. Therefore the peak in Fig. 5 should occur for $\Delta_d = 0$ and $P_d = 1065$ MeV/c, as it does.

The Monte Carlo calculation of the SM cross section reproduces quite well the shape and magnitude of the experimental results. This shows that the SM is the dominant mechanism within the phase space region that was investigated. The difference of about 10 MeV/c between the maximum of the experimental data and the maximum of the SM prediction is probably due to the uncertainty of the absolute field strength of the spectrometer magnet.

The fact that the calculated cross sections using the simple SM are consistently lower than the ex-

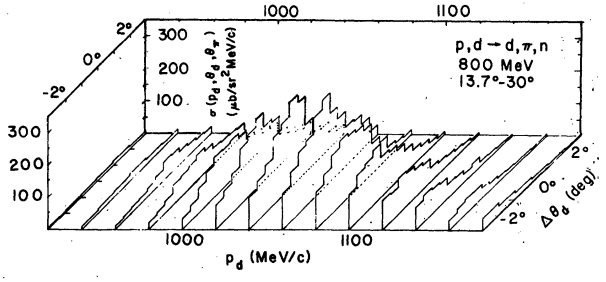

FIG. 6. The cross section $\sigma(P_d, \theta_d, \theta_\pi)$ as a function of deuteron momentum and angle for the $pd \rightarrow d\pi^+ n$ reaction at 800 MeV. Error bars are not shown.

perimental data at higher momentum transfer suggests that other mechanisms such as those shown in Figs. 2(g) and 2(f) contribute noticeably in these regions. These processes might be taken into account by distorting the wave functions in the incident channel, or using the method of Glauber double scattering.[20] Neither method has been attempted at present. These processes should become more important as P_n increases.

The results of the analysis in the cases where P_n cannot be zero are given in Table II and Fig. 7. Again, the angular average of the $\sigma(P_d, \theta_d, \theta_\pi)$ spectrum was a maximum at a P_d for which the corresponding P_n is a minimum. Figure 7 also shows the comparison of SM with the experimental data. The shapes of the data are reproduced, however, the magnitude of the SM increasingly deviates from the data as the minimum neutron recoil momentum increases from $P_n = 10$ to 100 MeV/c. This was also observed in Ref. 11 where the data were obtained at minimum $P_n > 400$ MeV/c and the SM values are found to be about one-tenth of the experimental data.

To determine the quality of the SM prediction, the theoretical calculation was normalized to the data. The value of the normalization N is shown in Table III. The normalization was obtained by minimizing $\chi^2 = \sum[(\mathrm{Exp}_i - N \cdot SM_i)/\Delta_i]^2$ for each angle setting individually. However, the reduced chi squares of the normalizations are greater than 10 in most cases, indicating that an additional term with different momentum dependence is needed to fit the data.

V. CONCLUSION

The $pd \to d\pi^+ n$ reaction at 800 MeV has been studied under various kinematic conditions. It was observed that the reaction basically proceeds through a quasifree process with a neutron spectator in the regions of phase space that were studied. It was noted that the simple spectator model predicts the magnitude of the observed cross section near the region where the neutron momentum P_n

TABLE II. Tabulated values of the cross section as a function of deuteron momentum and angle for the reaction $pd \to d\pi n$ at 800 MeV. The angles of the detector arms do not satisfy kinematics for the reaction $pp \to d\pi$. The symbols are the same as in Table I except $P_{\min}$ represents the minimum spectator momentum.

θ_M/θ_T	15°/30°		15°/40°		15°/50°	
$P_{\min}$	21 (MeV/c)		8.1 (MeV/c)		13.6 (MeV/c)	
P_d at $P_{\min}$	1040 (MeV/c)		1149 (MeV/c)		1234 (MeV/c)	
	Exp	SM	Exp	SM	Exp	SM
P_d (MeV/c)	(μb/sr^2-MeV/c)		(μb/sr^2-MeV/c)		(μb/sr^2-MeV/c)	
900	5.35 ± 0.87	2.82				
920	9.38 ± 1.2	5.59				
940	17.8 ± 1.6	11.3				
960	36.4 ± 2.3	21.8				
980	54.9 ± 2.9	40.9	1.08 ± 0.30	0.81		
1000	97.6 ± 4.0	70.8	2.45 ± 0.44	1.71		
1020	133.0 ± 4.8	107	5.06 ± 0.63	3.37		
1040	147.0 ± 5.1	134	10.6 ± 0.93	7.19	0.72 ± 0.22	0.12
1060	127.0 ± 4.7	135	14.1 ± 1.1	14.2	0.80 ± 0.27	0.28
1080	100.0 ± 4.2	106	29.3 ± 1.6	27.5	1.53 ± 0.33	0.55
1100	55.6 ± 3.2	67.3	51.4 ± 2.2	48.2	2.20 ± 0.40	1.23
1120	35.8 ± 2.5	40.4	77.3 ± 2.8	74.7	3.56 ± 0.51	2.61
1140	17.4 ± 1.8	21.6	97.6 ± 3.2	92.2	8.69 ± 0.79	5.55
1160	12.0 ± 1.5	11.5	89.3 ± 3.1	88.6	15.3 ± 1.1	11.9
1180			67.9 ± 2.7	62.2	28.5 ± 1.5	23.9
1200			42.0 ± 2.1	36.7	44.9 ± 2.0	40.6
1220			20.4 ± 1.5	18.2	65.7 ± 2.5	55.4
1240			13.5 ± 1.2	9.01	37.1 ± 2.4	53.6
1260			6.91 ± 0.88	4.28	36.2 ± 1.9	35.9
1280			2.73 ± 0.56	2.22	17.7 ± 1.3	17.3
1300					10.1 ± 0.97	8.37
1320					4.60 ± 0.67	3.50
1340					2.59 ± 0.50	1.79
1360					0.88 ± 0.30	0.88

TABLE II. (*Continued*).

θ_M/θ_T	17.5°/30°		20°/40°		17.5°/40°		17.5°/50°	
P_{min}	62.5 (MeV/c)		95.6 (MeV/c)		51.2 (MeV/c)		59.3 (MeV/c)	
P_d at P_{min}	1013 (MeV/c)		1087 (MeV/c)		1114 (MeV/c)		1200 (MeV/c)	
P_d (MeV/c)	Exp (μb/sr^2-MeV/c)	SM	Exp (μb/sr^2-MeV/c)	SM	Exp (μb/sr^2-MeV/c)	SM	Exp (μb/sr^2-MeV/c)	SM
820	0.58 ± 0.16	0.16						
840	0.85 ± 0.19	0.31						
860	1.59 ± 0.25	0.62						
880	2.46 ± 0.32	1.17						
900	4.60 ± 0.43	2.21	0.31 ± 0.08	0.06				
920	7.36 ± 0.55	4.06	0.46 ± 0.10	0.11				
940	11.5 ± 0.70	7.28	0.68 ± 0.12	0.19	0.87 ± 0.19	0.23		
960	20.2 ± 0.94	13.6	1.40 ± 0.16	0.37	1.60 ± 0.26	0.48		
980	28.3 ± 1.2	20.5	1.58 ± 0.18	0.64	2.14 ± 0.30	0.89		
1000	38.6 ± 1.4	30.6	2.72 ± 0.23	1.08	2.54 ± 0.33	1.87		
1020	41.4 ± 1.4	36.4	4.01 ± 0.28	1.94	6.86 ± 0.55	3.52	0.56 ± 0.21	0.07
1040	35.0 ± 1.3	33.3	5.36 ± 0.33	2.98	10.5 ± 0.68	6.52	0.72 ± 0.24	0.15
1060	26.5 ± 1.2	25.2	6.83 ± 0.38	4.66	16.2 ± 0.85	11.5	1.70 ± 0.37	0.30
1080	16.7 ± 0.92	15.4	8.45 ± 0.43	5.89	28.4 ± 1.2	21.9	1.36 ± 0.33	0.61
1100	8.88 ± 0.68	7.94	6.31 ± 0.36	5.57	39.9 ± 1.4	30.3	2.89 ± 0.48	1.17
1120	5.80 ± 0.56	4.24	5.13 ± 0.34	4.41	46.7 ± 1.6	36.8	3.71 ± 0.55	2.29
1140	2.82 ± 0.40	2.37	3.51 ± 0.28	3.00	40.7 ± 1.5	33.4	6.60 ± 0.75	4.49
1160	1.86 ± 0.33	1.36	1.72 ± 0.20	1.80	27.5 ± 1.2	20.5	12.4 ± 1.1	7.76
1180			1.05 ± 0.16	1.01	15.1 ± 0.92	11.3	14.9 ± 1.2	11.1
1200			0.40 ± 0.10	0.52	9.31 ± 0.73	5.47	15.9 ± 1.3	12.7
1220			0.40 ± 0.10	0.30	3.65 ± 0.45	2.55	14.2 ± 1.2	10.6
1240					2.24 ± 0.37	1.38	9.59 ± 1.0	6.74
1260					1.22 ± 0.28	0.74	4.07 ± 0.66	3.57
1280							3.37 ± 0.62	1.78
1300							1.29 ± 0.30	0.89

equals 0. The SM calculation drops to 35% of the observed strength of the reaction as the minimum P_n increases to 100 MeV/c, and other processes will be required to give the correct magnitude.

Apparently what is needed is an additional weakly momentum dependent background since the shapes of the spectra are well represented by the $pp \to d\pi^+$ process. Distortion of waves in the incident channel or the double scattering calculations of Duck *et al.*[20] may provide this additional strength. These more complicated models have not been included in the present analysis because the amplitudes involved vary rapidly over the solid angle and momentum acceptance of the detectors. Therefore, to correctly compare a theoretical calculation to the data the calculation must be averaged over these variables which requires extensive computer time. Cross sections measured under kinematic conditions where the spectator momentum is near the Fermi momentum are important, however, in understanding the roles that single and double scattering processes play in the overall amplitude. It is in this range of spectator momentum that interference between the two processes is expected.

Finally, we note that in this particular channel the quasifree process is a valid approximation. This leaves open the question presented by the data of Cochran *et al.*[9] Simple Glauber shadowing is ruled out because it would affect all quasifree exit channels equally and the SM is valid for the present experiment. Also, as was pointed out in the introduction, Eq. (1) cannot predict the magnitude of the observed effect. Interference between the amplitudes proceeding through $pp \to \Delta^{++}n$ and $pn \to \Delta^+ n$ in a quasifree manner is possible, though it has been shown that the free amplitudes for $pp \to \Delta^{++}n$ and $pp \to \Delta^+ p$ do not interfere significantly because they contribute predominantly in different spin states.[31] Since both the neutron and proton are in the same spin state within the deuteron, one might also expect that the $pp \to \Delta^{++}n$ and $pn \to \Delta^+ n$ amplitudes would not interfere.

The pion spectrum for the reaction $pd \to \pi^+ X$ will

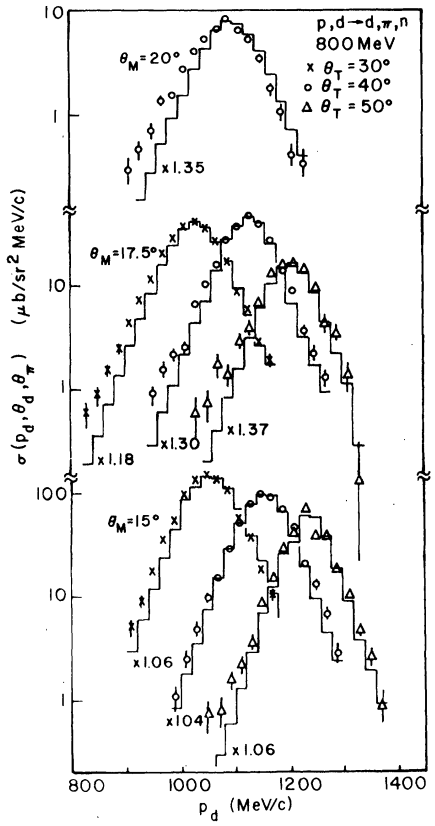

FIG. 7. The cross section $\sigma(P_d\,\theta_d\,\theta_\pi)$ as a function of deuteron momentum for angles that do not satisfy the kinematics for the reaction $pd \to d\pi$. The solid lines are the SM predicted values.

be spread in energy and angle due to the Fermi motion of the nucleons. However, for a broad resonance such as the (3,3) resonance, which dominates pion production amplitudes in the central region of the pion spectrum, the Fermi averaged spectrum should not change appreciably. At the higher end of the spectrum where the quasi-free reactions $pp \to d\pi$ and $pp \to (NN)\pi$ contribute, this effect is more important. In this case the Fermi momentum will spread the pion spectrum into the (3,3) resonance structure and the quasi-free peak may be too broad to be observed. This effect could account for at least some of the missing strength.

TABLE III. The normalization factor N obtained by a χ^2 normalization of the SM to the data. The symbol P_n is the spectator recoil momentum.

P_n (MeV/c)	θ_M/θ_T	N
0	13.7/20.4	0.92
0	13.7/25	1.01
0	13.7/30	1.02
0	13.7/35	1.02
0	13.7/40	1.04
0	14.7/45	1.09
8.1	15/40	1.04
13.6	15/50	1.06
21.0	15/30	1.06
51.2	17.5/40	1.30
59.3	17.5/50	1.37
62.5	17.5/30	1.18
95.6	20/40	1.35

Inclusive pion production at 800 MeV from several targets including hydrogen and deuterium is now under analysis by this group to check the results of Ref. 9. The differences in strength of the pion production from hydrogen and deuterium is not well publicized, but its solution may be extremely important in understanding the spin dependent pion production amplitudes from nuclei.

ACKNOWLEDGMENTS

It is a pleasure to acknowledge several valuable discussions with Dr. I. Duck concerning this work. This research was supported in part by the U. S. Department of Energy under Contracts No. EY-76-S-05-3948 and No. EY-76-C-05-1316.

[1]C. Richard-Serre *et al.*, Nucl. Phys. B20, 413 (1970).
[2]B. M. Preedom *et al.*, Phys. Lett. 65B, 31 (1976).
[3]R. D. Felder, Ph.D. thesis, Rice University (unpublished).
[4]R. M. Heinz, O. E. Overseth, D. E. Pellett, and M. L. Perl, Phys. Rev. 167, 1232 (1968).
[5]H. L. Anderson *et al.*, Phys. Rev. D 9, 580 (1974).
[6]W. Dollhopf *et al.*, Nucl. Phys. A217, 381 (1973).
[7]E. Aslanides *et al.*, Phys. Rev. Lett. 39, 1654 (1977).
[8]K. R. Hogstrom *et al.*, Phys. Rev. C 17, 259 (1978).
[9]D. Cochran *et al.*, Phys. Rev. D 6, 3085 (1972).
[10]D. O. Riska, M. Brack, and W. Weise, Phys. Lett. 61B, 47 (1976).
[11]D. S. Koltun, Adv. Nucl. Phys. 3, 71 (1969).
[12]G. A. Miller, Nucl. Phys. A223, 477 (1974).
[13]M. Ruderman, Phys. Rev. 87, 383 (1952).
[14]C. Ingram, N. W. Tanner, J. J. Domingo, and J. Rohlin, Nucl. Phys. B31, 331 (1971).
[15]G. Barry, Phys. Rev. D 7, 1441 (1973).
[16]V. Basin and I. Duck, Phys. Lett. 46B, 309 (1973).
[17]H. Fearing, Phys. Rev. C 11, 1210 (1975).
[18]H. Fearing, Phys. Rev. C 11, 1495 (1975).
[19]A. M. Green and E. Maqueda, University of Helsinki report (unpublished).

[20]I. Duck, K. R. Hogstrom, and G. S. Mutchler, Phys. Rev. C 17, 259 (1978).
[21]T. Witten *et al.*, Nucl. Phys. A254, 269 (1975).
[22]B. E. Bonner, private communication.
[23]R. Silbar, private communication.
[24]Cryogen, Inc., Cryodyne Helium Refrigerator Model 1020.
[25]J. A. Buchanan, Rice University (unpublished).
[26]H. Jones *et al.*, IEEE Trans. Nucl. Sci. 20, 691 (1973).
[27]J. A. Buchanan and H. Jones, IEEE Trans. Nucl. Sci. 19, 682 (1972).
[28]M. J. Moravsick, Nucl. Phys. 7, 113 (1958).
[29]T. M. Williams, Ph.D. thesis, Rice University (unpublished).
[30]H. B. Willard *et al.*, Phys. Rev. C 14, 1545 (1976).
[31]I. Duck, private communication.